Powder Technology 405 (2022) 117506

Contents lists available at ScienceDirect

Powder Technology

journal homepage: www.elsevier.com/locate/powtec

A model for predicting the performance of a batch fountain confined spouted bed dryer at low and moderate temperatures

Xabier Sukunza [a,*], Aitor Pablos [b], Mikel Tellabide [a], Idoia Estiati [a], Fábio Bentes Freire [c], Roberto Aguado [a,b], Martin Olazar [a,b]

[a] Dept. of Chemical Engineering, University of the Basque Country UPV/EHU, PO Box 644, E48080 Bilbao, Spain
[b] Spouted Bed Solutions, Ltd., Zitek Leioa, Rector's Building, Biscay Campus, Ground Floor, Sarriena, E48940 Leioa, Spain
[c] Department of Chemical Engineering, Federal University of São Carlos, Via Washington Luis, km235, P.O. Box 676, 13565-905 São Carlos, SP, Brazil

ARTICLE INFO

Article history:
Received 11 February 2022
Received in revised form 4 May 2022
Accepted 10 May 2022
Available online 14 May 2022

Keywords:
Simulation
Conical spouted bed
Drying
Fountain confiner
Mass transfer coefficient

ABSTRACT

Spouted bed dryers are well known for their high efficiency at low and moderate temperatures. The design of industrial scale dryers requires the estimation of heat and mass transfer coefficients, but there is hardly any information involving their estimation in fountain confined conical spouted beds. Thus, a model is proposed for predicting their performance, which is based on unsteady state heat and mass balances for the solid and air phases in the spout, fountain and annulus. It was validated by comparing the output values with those obtained in previous batch drying runs, and therefore allows predicting the dryer performance and the mass transfer coefficient. The results show that the temperature and velocity of the air at the inlet, as well as the solid properties, are highly influential parameters, which is explained by the level of turbulence attained. Therefore, this model allows predicting the performance of industrial spouted bed dryers.

1. Introduction

Since the spouted bed was developed by Mathur and Gishler [1] for wheat drying (Geldart D particles), numerous studies have been reported concerning drying [2–6], combustion [7–10], pyrolysis [11–15], torrefaction [16] and coating [17,18], among others. Given the high rates of particle circulation and heat and mass transfer, and the simplicity of the equipment, spouted beds have become a promising alternative to fixed and fluidized beds. In fact, they have been extensively used for drying, since this operation involves the removal of water from wet materials in a wide range of applications, as are those related to pharmaceutical, chemical, food and mining industries. Thus, drying allows reducing transportation costs, as well as inhibiting biological reactions that take place in the presence of moisture.

There are several studies in the literature concerning drying of grains [19,20], coarse [21] and fine particles [22,23], pastes and suspensions [24,25], and slurries [26,27]. However, few of them approach drying modelling, which may be due to the complexity involving a correct mathematical description of the physical phenomena occurring in the drying chamber, namely those involving hydrodynamics and heat and mass transfer. Most of the studies are based on developing a macroscopic bed model to solve the heat and mass balances in the bed. Accordingly, several authors [28–31] have developed models assuming thermal equilibrium between the solid and the exiting air, which accounts for their simplicity. However, although they allow reasonable predictions of solid moisture content under certain conditions, do not account for temperature changes in the bed during the falling rate period or when drying rate is not constant. Therefore, heat balances must be considered in any rigorous model in order to predict the evolution of drying throughout time. Accordingly, Madhiyanon et al. [32] developed a model for batch drying of grains assuming that neither thermal equilibrium was reached nor temperature was constant. The model was validated by using experimental data obtained in a two dimensional spouted bed dryer. Markowski et al. [33] also assumed a non-isothermal process for the drying of barley. They studied the influence of grain shape on water diffusivity across the particle. Moreover, Bie et al. [34] and Go et al. [35] proposed a model for the drying of wheat in a triangular spouted bed. Although they did not assume thermal equilibrium, a poor agreement was found in grain temperature.

Furthermore, the drying of suspensions using inert particles has also gained great attention in the food and chemical industry [36–38]. For instance, Oliveira et al. [39] and Moreira da Silva et al. [24] analysed the water evaporation rate in the spout, fountain and annulus using a three region model in a conical spouted bed, in which water was continuously fed as droplets onto an inert bed. Despite an overall good agreement was found, the powder moisture content was not accurately

* Corresponding author.
E-mail address: xabier.sukunza@ehu.eus (X. Sukunza).

https://doi.org/10.1016/j.powtec.2022.117506

predicted at high feed rates. Accordingly, the use of Artificial Neuronal Networks (ANN) has also been proposed to improve the modelling performance. Several authors have applied this method for predicting moisture and temperature in the drying of skimmed milk, blood, sewage sludge and a suspension of calcium carbonate [25,40,41]. Nevertheless, ANN modelling is not straightforward and, furthermore, a great amount of experimental data is required.

Although spouted bed drying has been applied in the mining industry [42,43], the greatest limitations of this technology lie in the operation stability when fine particles are used. Thus, the ratio between the gas inlet diameter and particle diameter, D_o/d_p, should be smaller than 20–30 in order to attain stable operation [44]. This limits the scaling up of spouted beds for its implementation in large-scale industrial applications. The use of draft tubes is a usual solution, which allows operating with Geldart B particles [45,46]. Thus, this internal device has been applied for the drying of yeast, barley and wheat grains [19]. Altzibar et al. [47] studied the effect of the draft tube in the drying of fine sand in a conical spouted bed and no instabilities were found during the runs. Olazar et al. [48] developed a three region drying model of a non-porous draft tube conical spouted bed and, although they did not assume thermal equilibrium, the heat balance in the bed was neglected. However, the model accurately predicted the solid moisture and air outlet humidity.

Although draft tubes allow treating fine and ultrafine particles in conical spouted beds, they reduce gas percolation from the spout into the annulus, thereby reducing the drying capacity of the spouted beds. Moreover, high fountains are attained, which leads to severe elutriation. The best solution to avoid this effect is the use of a fountain confiner [49], which retains the particles ascending through the spout and returns them back to the bed, avoiding particle elutriation [50]. Furthermore, it allows increasing the upper limit of the residence time of the air, improving the gas-solid contact, and consequently reducing the time required for drying [22]. This configuration was used in previous studies [23,51] and drying efficiencies of up to 95% were attained in continuous operation with fine and ultrafine sands.

Moreover, Tellabide et al. [52] operated with particles of 0.05 mm using the fountain confiner, but without any draft tube. This configuration allowed increasing the stability range to a D_o/d_p ratio of 800, which involved a huge step forward in the scaling-up of spouted beds. Other good indicators to consider when scaling up this process are the heat and mass transfer coefficients, since they are essential parameters in the design of industrial scale dryers. Although there are a few correlations in the literature for estimating mass transfer coefficients in standard spouted beds [53–55], there is no one for conical spouted beds (either plain or fountain confined). In fact, a few correlations refer to heat transfer coefficients and were proposed by Saldarriaga et al. [56] and Yaman et al. [57]. In order to overcome this lack of information, certain authors [58–61] recommend the determination of mass transfer coefficients in each region (spout, fountain and annulus) based on correlations proposed in the literature for packed, dilute and very dilute systems. Nevertheless, this approach does not seem to provide satisfactory results for designing spouted bed equipment for industrial applications [62]. A rigorous three region drying model based on heat and mass balances is proposed in this study, which is validated using experimental data obtained in a previous study [63], with the overall mass transfer coefficient being the sole fitting parameter.

2. Experimental

2.1. Materials and equipment

Two types of siliceous sands have been used, which are by-products in the production of kaolin in the mining industry. In order to conduct the physical characterization of the sands, 100 g samples were prepared using the quartering method (ISO 14488:2007 standard). The moisture content has been measured by the ISO-589 standard, which has also been confirmed in a HR83 halogen moisture analyser. The Sauter mean diameter (d_p^w) has been obtained by sieving 100 g of dried sample in a CISA RP 200 N with sieves of 50, 100, 200, 300, 400, 500, 630 and 800 μm. Fig. 1 shows the particle size distribution of the sands used. The volume average particle size (d_p^v) of the sands have been obtained by laser diffraction in a Mastersizer 2000, with the results being similar to those obtained by sieving. Accordingly, both sands are made of fine particles, and the average particle sizes are 196.6 μm (fine sand) and 47.7 μm (ultrafine sand). Particle density (ρ_s) has been measured with a pycnometer and distilled water following ISO 18753:2017 standard, and bed density (ρ_b) and shape factor (ϕ) have been measured following the indications by Brown and Richards [64]. The specific surface area of the sands (a) has been determined following the BET method (ISO 9277 standard) in a Micromeritics ASAP 2010. Table 1 summarizes the physical properties of both sands.

The drying experiments have been carried out in a pilot plant equipped with a conical spouted bed. Fig. 2 shows the elements of the unit, whose details have been reported in previous studies by our research group [23,51,63]. The main element of the pilot plant is the contactor, in which the drying takes place, and is made of stainless steel in order to allow operating at temperatures above the ambient one. The bed is located in the conical section, Fig. 3a, with its dimensions being as follows, Table 2: cone angle (γ), 32°, base diameter (D_i), 0.07 m, column diameter (D_c), 0.36 m, height of the conical section (H_c), 0.55 m, and air inlet diameter (D_o), 0.05 m. In order to allow stable operation in the drying chamber, two internal devices of stainless steel were used, namely draft tube and fountain confiner, whose dimensions have been optimized in previous papers by our research group [50,65] and are summarized in Table 2. Fig. 3b shows the draft tube, which has the following geometric dimensions: tube diameter (D_T), 0.05 m, distance between the air inlet nozzle and the lower end of the tube (L_H), 0.1 m, and aperture ratio (A_o/A_T), 60%. The total length of the draft tube (L_T) is the same as the bed height, 0.45 m. The fountain confiner has a total length (L_F) of 0.9 m and a diameter (D_F) of 0.2 m. The distance between the upper surface of the bed and the lower end of the fountain confiner (H_F) is 0.1 m, which is the optimum to ensure stable operation [50,66,67]. The schematic 3D representation of the contactor is shown in Fig. 4.

Air is supplied by a 4 kW RODE 500 blower, with a maximum flow rate of 300 $Nm^3\ h^{-1}$ and a pressure of 130 kPa. The air flow rate is measured by a vortex type flow meter, Powirl 77. The air is heated by a cartridge of electrical resistances (RXP E32348), which supply a maximum power of 7.5 kW. Both the blower and the heater are coupled to a PID controller. The elutriated fine particles are collected in a bag filter (AAF Fabri Pulse-L), and a 3 kW dryer booster fan drives the air from the contactor to the vent. The inlet and outlet humidity and temperature of the air, as well as bed temperature, are monitored for the validation of the model.

2.2. Drying procedure

Different operating conditions were used out in order to assess their influence on the drying performance and, specifically, on the mass transfer coefficient in a spouted bed dryer. Thus, three inlet air velocities were used, which are $u/u_{ms} = 1.2$, 2 and 3 ($u_{ms} = 5.66\ ms^{-1}$) in the drying of the fine sand and $u/u_{ms} = 1.2$, 1.5 and 2 ($3.40\ ms^{-1}$) in the drying of the ultrafine sand. Higher inlet air flow rates must not be used with the ultrafine sand due to excessive particle entrainment. Four inlet air temperatures were used in the runs, which are $T_i = 35$, 50, 100 and 150 °C.

Prior to any experimental run, the internal devices are placed in the empty contactor, as shown in Fig. 4. A 0.45 m bed height was selected based on the promising results obtained in previous studies by our research group in the continuous drying of sand [23,51]. This accounts for 21 and 19 kg of fine and ultrafine sand, respectively. Afterwards,

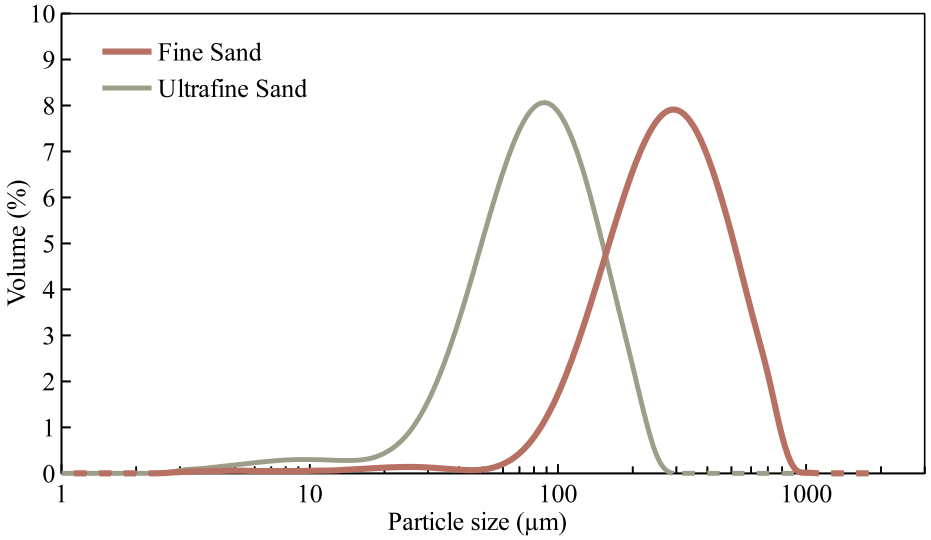

Fig. 1. Particle size distribution of the sands.

air is fed into the drying chamber at a given flow rate and temperature. Once the dry sand bed has reached the inlet air temperature and steady state is attained, a pulse of wet sand is injected into the reactor through the solid feeder above the bed surface, Fig. 4. The amount of this wet sand is 2.3 kg, which is made up of 2 kg of dry sand and 0.3 kg of water. Accordingly, the wet sand injected is a homogeneous mixture with a moisture content of 15 wt% on a dry basis. Therefore, there is a mass increase in the bed of 2.3 kg and the moisture is homogeneously distributed in the bed. Air flow rate, air temperature and humidity at the inlet and outlet, and bed temperature are monitored during the process. Drying has been considered to be finished when the outlet air temperature is close to the inlet one (5% difference at most). Each run has been repeated at least 3 times in order to ensure reproducible results.

3. Drying modelling

One of the main aims of this paper is to analyse the influence of the operating parameters on the mass transfer performance in a fountain confined conical spouted bed dryer. Since the determination of mass transfer coefficients is not straightforward, a mathematical model has been built based on unsteady state heat and mass balances in the drying chamber and validated using the experimental data corresponding to batch runs. The sole fitting parameter of the model is the overall mass transfer coefficient. Although certain authors considered that shallow spouted beds behave as perfectly mixed tanks [68], previous drying simulations under this assumption show that the calculated values do not match the experimental ones [69]. Therefore, following a common methodology in the literature [35,39,48,70], a three region model has been proposed in this paper, which describes the air and solid circulation in the spout, fountain and annulus of spouted beds. It should be noted that approaches based on CFD have also been used recently for the prediction of particle hydrodynamics [71,72].

Table 1
Physical properties of the sands.

Parameter	Fine sand	Ultrafine sand
d_p^w (μm)	196.6	47.7
d_p^v (μm)	303.1	70.8
ρ_s (kg m^{-3})	2150	2300
ρ_b (kg m^{-3})	1576	1385
ϕ	0.7	0.7
a (m^2 kg^{-1})	157.8	607.9
Geldart type	*B*	*A*

As well known, the air is introduced into the spout bottom, rises to the fountain, and finally leaves the contactor through the outlet pipe. Furthermore, part of the inlet flow rate diverts into the annulus, especially at the bottom section, but diversion may also occur along the whole spout when there is no draft tube [73] or operation is carried out using an open-sided draft tube [74]. In these cases, the air rises also along the annulus and joins that coming from the fountain at the top of the bed. The solid, however, is introduced into the upper surface of the annulus. It then goes down through this zone, at the same time as there is cross-flow into the spout, especially close to the bottom of the bed. The solid incorporated into the spout rises to the fountain and falls back onto the annulus. Although the role of the different regions of the spouted bed in the drying of particulate materials remains a subject of discussion, the drying of non-porous small-sized particles, as those used in this study, occurs mainly in the spout [24,48]. Accordingly, this region has been divided into two compartments or nodes.

As previously mentioned, a fountain confiner has been used in this study, and therefore considered in the model. In fact, the fountain region is the volume within the confiner. Furthermore, the volume of the fountain confiner is approximately two times the volume of the conical section, and this region has a voidage of around 0.90, as well as high

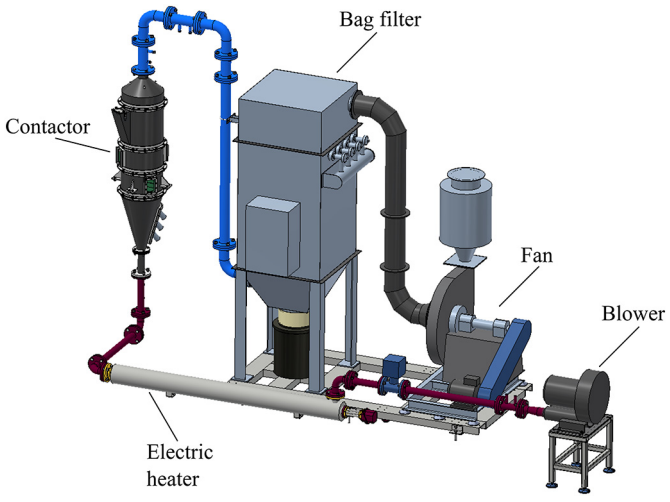

Fig. 2. Schematic representation of the spouted bed based pilot plant.

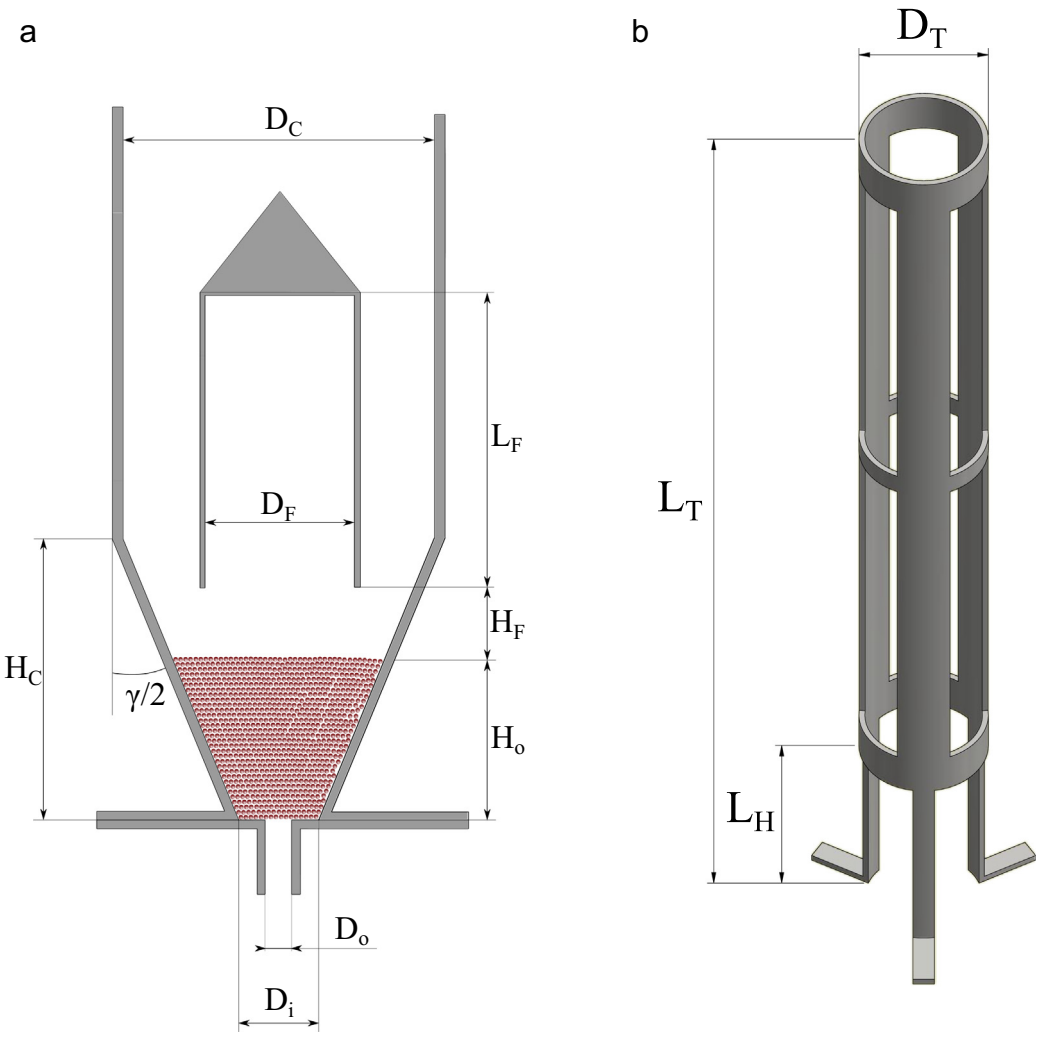

Fig. 3. Geometric factors of (a) the conical spouted bed and (b) the draft tube.

turbulence. Accordingly, a single node has been proposed in this region. The annulus has also been considered as a single node, since the air reaches thermal equilibrium in this region, especially in shallow beds [75]. This is a new aspect that has not been considered in the literature and clearly allows simplifying the model. Fig. 5 shows a diagram of the proposed model. Each node behaves like a perfectly mixed stirred tank.

Table 2
Dimensions of the contactor and internal devices.

Geometric parameter	Value
Contactor	
γ(°)	32
D_i (m)	0.07
D_c (m)	0.36
H_c (m)	0.55
D_o (m)	0.05
Draft tube	
D_T (m)	0.05
L_H (m)	0.1
A_o/A_T (%)	60
L_T (m)	0.45
Fountain confiner	
L_F (m)	0.9
D_F (m)	0.2
H_F (m)	0.1

Although the annulus is often considered as a plug flow in the literature, the use of an open sided draft tube allows solid cross-flow from the annulus into the spout all over the spout. Therefore, this region may also be considered as a single node with mixed flow. A fraction of the air fed through the bottom inlet diverts into the annulus, where the particles descend. According to several authors [46,77–81], the air percolation from the spout into the annulus depends on bed height, particle diameter and height of the entrainment zone in the draft tube. We have measured the air flow rate on the upper surface of the annulus by means of an anemometer [48] and accounts for approximately 10% of the total air flow rate at the inlet for beds made up of either fine or ultrafine sand. Furthermore, preliminary simulations have shown that changes in the 5% to 15% range hardly affect the predictions for the drying performance of the materials studied. Therefore, the fraction of air diverted into the annulus was kept constant at 10% for both fine and ultrafine sand under all the conditions studied. This low air diversion into the annulus is especially due to the low particle size, and therefore the low permeability in this zone.

3.1. Heat and mass balances

The mass balance of water in the solid phase contained in any node defined in the spouted bed is described by Eq. (1). Although particle shrinkage and water diffusion within the particles are commonly considered in drying modelling [82], given the small particle size and

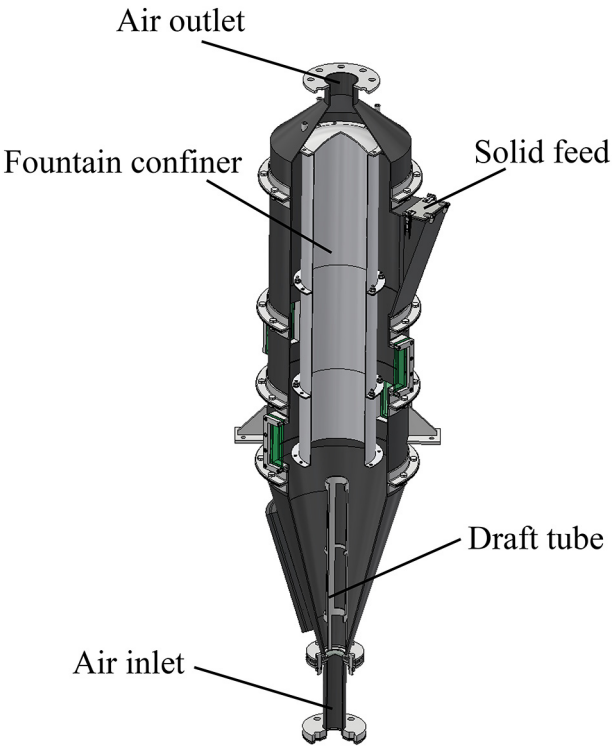

Fig. 4. Schematic 3D view of the spouted bed configuration used for the drying of sands.

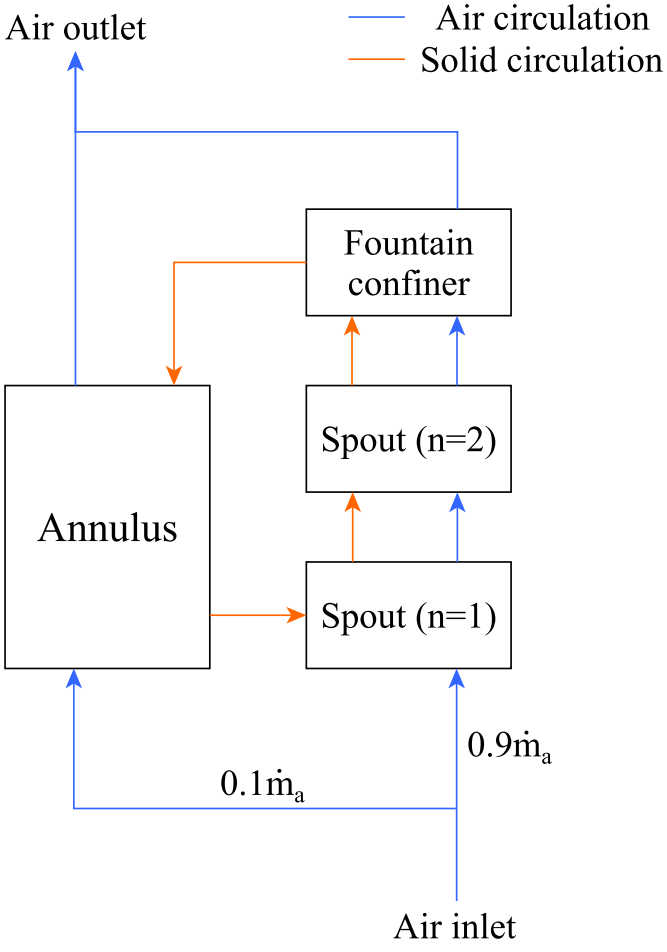

Fig. 5. Diagram of the proposed drying model.

their low specific surface area, both mechanisms are negligible. The evolution of the water content in each node is a consequence of the flow rate coming from the previous node, the flow rate leaving the node and the water evaporation rate. The superscript i stands for the node to which the balance is carried out and j for the previous one. Thus, in the first node of the spout, j corresponds to the whole annular region (previous node) and, in the second node of the spout, it corresponds to the first node in the spout. In the fountain, j corresponds to the second node in the spout, and in the annulus to the fountain region.

$$M_s^i \frac{dx_s^i}{dt} = \dot{m}_s\left(x_s^j - x_s^i\right) - R_w^i M_s^i \tag{1}$$

In this equation, x_s is the moisture content of the solid, M_s is the amount of dry sand in the node, and $\dot{m}_s$ is the solid circulation mass flow rate in the bed, which can be estimated based on the bed mass and the solid cycle time [83–85], by means of artificial neural networks [81] and empirical correlations [82]. Moreover, it can be experimentally measured following the methodology described by Estiati et al. [86]. The effect of the solid wetness is negligible due to the low water content in the bed during the drying process, and therefore solid circulation mass flow rate is assumed to be constant during the drying process. Thus, for 21 kg of fine sand and 19 kg of ultrafine sand, the solid circulation mass flow rates are 2.5 and 2.0 kg s^{-1}, respectively. R_w is the drying rate, which is calculated by means of the mass transfer coefficient, as explained in the following section. The mass of dry sand in any node is calculated based on the node volume and porosity and particle density, as follows:

$$M_s^i = \left(1 - \epsilon^i\right) V^i \rho_s \tag{2}$$

In Eq. (2), ϵ is the porosity of the corresponding node, i.e., 0.4, 0.6 and 0.9 in the annulus, spout and fountain, respectively. These values have been proposed based on a previous paper [87] and have been experimentally validated with the image recording system described in two recent papers [88,89]. The volume of the spout region is calculated assuming a cylinder whose diameter is the average diameter of the spout, which is estimated by the methodology reported by Tellabide et al. [88], and its length is the bed height, H_o. Moreover, the volume of the annulus is that corresponding to the conical section minus the spout region, and the volume of the fountain is that of a cylinder (confiner) whose diameter is D_F and length L_F.

Given the small size of the sand particles used and their low porosity, the outer layer surrounding the particles controls the heat transfer; that is, temperature may be assumed uniform in the whole particle [90]. Accordingly, the energy balance is given by the following equation:

$$\begin{aligned} M_s^i \frac{d}{dt}\left(h_s^i + x_s^i h_w^i\right) = \dot{m}_s\left(h_s^j + x_s^j h_w^j\right) - \dot{m}_s\left(h_s^i + x_s^i h_w^i\right) \\ + h_c^i a M_s^i \left(T_g^i - T_s^i\right) - R_w^i M_s^i h_v^i \end{aligned} \tag{3}$$

In Eq. (3), the terms on the right hand side account for the rates of energy input and output due to the wet solid flow rates entering and leaving the node, the heat transfer by convection from the hot gas phase to the solid particles and the loss of heat due to moisture evaporation during the drying. Furthermore, h_s, h_w and h_v are the specific enthalpies of the solid, water and steam, respectively, h_c is the heat transfer coefficient between the hot air and the solid. For estimating h_c in the high voidage spout and fountain regions, an appropriate equation is that by Rowe and Claxton [91], whereas in the low voidage annulus this heat transfer coefficient is calculated by the correlation proposed by Saldarriaga et al. [56]. Writing the enthalpies in Eq. (3) as functions of temperature, the evolution of solid temperature with time is calculated as follows:

$$\frac{dT_s^i}{dt} = \frac{1}{C_{p,s} + x_s^i C_{p,w}} \left(\frac{\dot{m}_s}{M_s^i} \left(h_s^j + x_s^j h_w^j - h_s^i - x_s^i h_w^i \right) + h_c^i a \left(T_g^i - T_s^i \right) - R_w^i h_v^i - h_w^i \frac{dx_s^i}{dt} \right) \quad (4)$$

Although the solid describes cycles in the spouted bed dryer, the hot air is continuously introduced from the gas inlet nozzle. Accordingly, the mass balance of the water in the air is given by the following equation:

$$M_g^i \frac{dy_g^i}{dt} = \omega \dot{m}_a \left(y_g^j - y_g^i \right) + R_w^i M_s^i \quad (5)$$

In Eq. (5), M_g is the mass of air in each node, y_g is the air absolute humidity, ω is the fraction of air diverted into the annulus ($\omega = 0.1$ in the annulus and 0.9 in the spout and fountain) and $\dot{m}_a$ is the total air mass flow rate. As in the mass balance, i superscript stands for the node to which the heat balance is carried out and j to the previous one. The mass of air in each node is determined based on the node features (volume and voidage) and air density,

$$M_g^i = \epsilon^i V^i \rho_s \quad (6)$$

Concerning the heat balance for the air in each node, the rate of accumulation of energy is a consequence of the rates of energy input and output due to the air flow rates entering and leaving the node, the heat loss by convection from the hot gas to the solid particles, the gain of heat due to the steam flowing from the particles into the air and the loss of heat through the wall to the ambient,

$$M_g^i \frac{d}{dt} \left(h_g^i + y_g^i h_v^i \right) = \omega \dot{m}_a \left(h_g^j + y_g^j h_v^j - h_g^i - y_g^i h_v^i \right) - h_c^i a M_s^i \left(T_g^i - T_s^i \right) + R_w^i M_s^i h_v^i - U_o A_o \left(T_g^i - T_{amb} \right) \quad (7)$$

The parameter U_oA_o in Eq. (7) is the overall coefficient for the heat transfer through the wall, and has been calculated for each run by solving the steady state heat balance in the spouted bed dryer containing dry sand (prior to feeding the wet sand). Its value ranges from 17.748 to 35.579 W ° C^{-1}, which is due to the different inlet air temperatures used in the drying runs. Furthermore, the heat transfer from the bed to the ambient through the wall only applies in the annulus section. Rearranging Eq. (7) with the mention considerations yields the explicit equation for determining the evolution of the air temperature with time:

$$\frac{dT_g^i}{dt} = \frac{1}{C_{p,g} + y_g^i C_{p,v}} \left(\frac{1}{M_g^i} \left(\omega \dot{m}_a \left(h_g^j + y_g^j h_v^j - h_g^i - y_g^i h_v^i \right) - h_c^i a M_s^i \left(T_g^i - T_s^i \right) + R_w^i M_s^i h_v^i - U_o A_o \left(T_g^i - T_{amb} \right) \right) - h_v^i \frac{dy_g^i}{dt} \right) \quad (8)$$

Although the model allows calculating the solid and air properties in each node, the values registered in the experimental runs are the air humidity and temperature at the outlet pipe located in the upper zone of the spouted bed dryer. Thus, the air leaving the fountain confiner joins that leaving the annulus and the whole stream leaves the dryer through the pipe located on top. Accordingly, heat and mass balances are carried out at the mixing point to determine the theoretical outlet values to be compared with the experimental ones:

$$\dot{m}_a y_g^{out} = \omega^A \dot{m}_a y_g^A + \omega^F \dot{m}_a y_g^F \quad (9)$$

$$\dot{m}_a \left(h_g^{out} + y_g^{out} h_v^{out} \right) = \omega^A \dot{m}_a \left(h_g^A + y_g^A h_v^A \right) + \omega^F \dot{m}_a \left(h_g^F + y_g^F h_v^F \right) \quad (10)$$

The air and solid properties required in the heat and mass balances, have been estimated based on theoretical and empirical correlations, Table 3.

Table 3
Equations used for calculating air and water properties.

Parameter	Equation
Air density (ρ_g)	$P = \frac{RT_g}{v-b} - \frac{a}{v^2+bv}$
Air dynamic viscosity (μ_g)	$\mu_g = \mu_0 \left(\frac{a}{b}\right) \left(\frac{T_g}{T_0}\right)^{3/2}$
Water vapour pressure (P_v)	$\log_{10} P_v = A - \frac{B}{T_g + C}$
Heat capacity (C_p)	$C_p = A + BT_g + CT_g^2 + DT_g^3 + \frac{E}{T_g^2}$
Air velocity (u_g)	$u_g = \frac{\lvert\rho_g\rvert_{T_{amb}}}{\lvert\rho_g\rvert_{T_g}} \frac{4Q}{\pi D_o^2}$
Heat conductivity (k_g)	$k_g = k_{T_0} \left(\frac{T_g}{T_0}\right)^{0.9}$

3.2. Drying rate

As stated above, given the small size of the sand particles used and their low porosity, the rate-limiting step in the drying process is the evaporation of water on their surface. According to the two-film theory, the drying rate may written as a function of the overall gas phase mass transfer coefficient and the corresponding driving force, as follows:

$$R_w^i = Ka \left(y_{sat} - y_g^i \right) \lvert\rho_g\rvert_{T_g^i} \quad (11)$$

In Eq. (11), gas density, ρ_g, depends on temperature, T_g, which changes from point to point in the bed. Thus, the vertical bars with gas temperature as subscript mean that gas density must be calculated at the temperature corresponding to i node. K is the overall gas phase mass transfer coefficient, a the interface area, y_{sat} and y_g are the saturation and actual air absolute humidities, and ρ_g the air density at the temperature in the node. Initially, there is water on the whole particle surface, i.e., the specific surface area of the particle, a, may be used as the interface area. However, as drying proceeds, the water on the surface of the particle evaporates until the critical moisture content, x_s^c, is reached. At this point, the moisture on the outer particle surface has been fully evaporated and the evaporation of the internal water begins. In fact, a sharp decrease in the outlet air humidity is observed in the experimental runs. Given the small size of the particles, this decrease is commonly attributed to the decrease in the gas/solid interface area, which can be determined by the characteristic drying curve of the particles [92]. Therefore, knowledge of the critical solid moisture content is essential for the application of this methodology, which differs depending on the solid properties. The values of this parameter determined for the fine and ultrafine sand particles are 0.26 and 0.42 wt% d.b., respectively. In the drying of fine and ultrafine sands, the interphase area is defined based on the shape of the characteristic drying curve determined experimentally:

$$\begin{cases} x_s \geq x_s^c \rightarrow a = a \\ x_s < x_s^c \rightarrow a = a \left(\frac{x_s}{x_s^c} \right)^3 \end{cases} \quad (12)$$

3.3. Optimization of the mass transfer coefficient

Fig. 6 outlines the algorithm written in Scilab (version 6.0.2) developed in order to solve the ordinary differential equations of the model. Thus, the algorithm uses the *ode* subroutine based on the *stiff* method for the integration of Eqs. (1), (5), (4) and (8). Moreover, the *fminsearch* subroutine based on the algorithm developed by Nelder and Mead [93] has been used for minimizing the objective function and finding the mass transfer coefficient of best fit to the experimental results. Concerning the initial conditions, the water content of the solid at the beginning of the drying process is that corresponding to the homogenized bed in all the nodes, as the wet sand is fed from the top and the bed

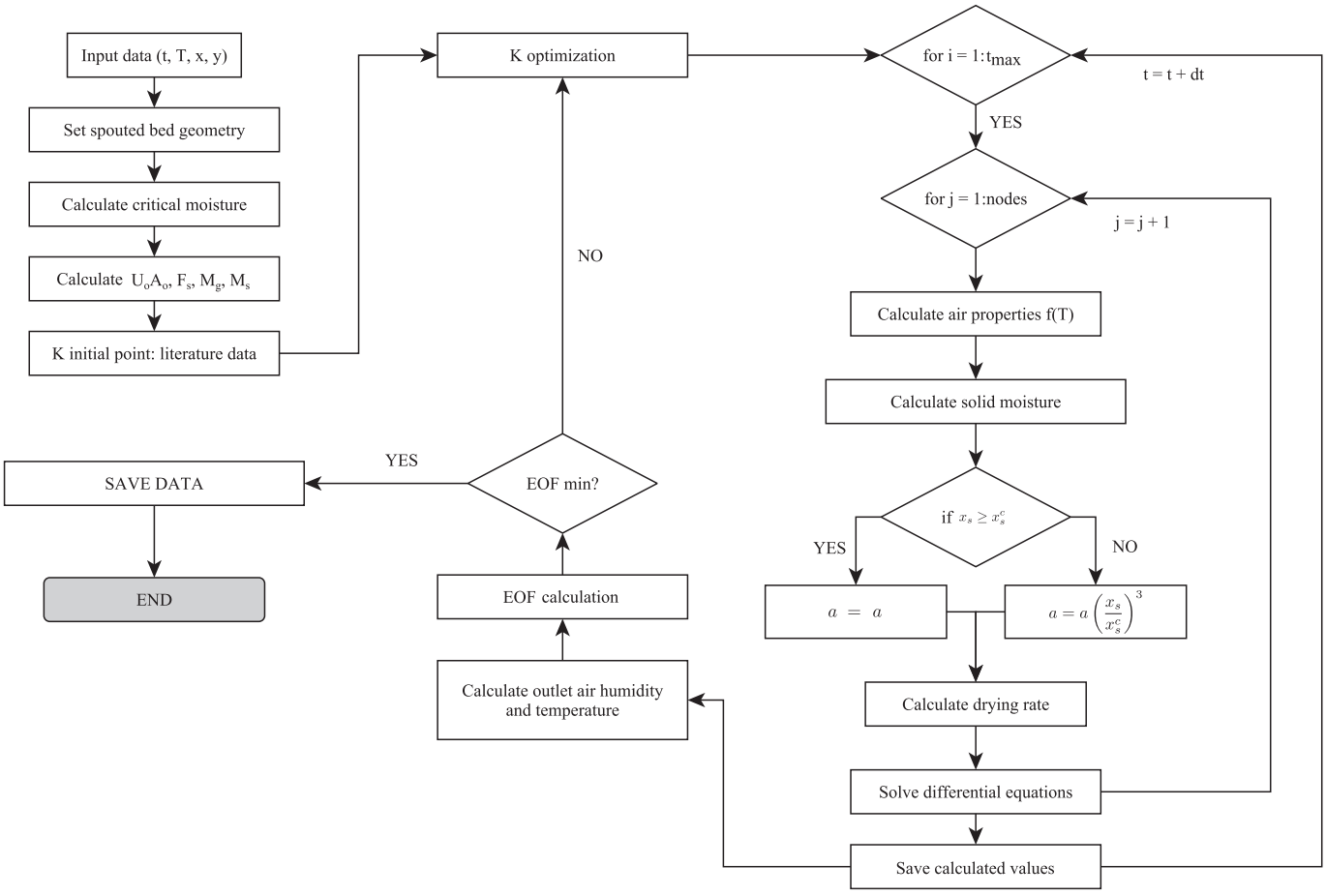

Fig. 6. Flowchart of the algorithm developed for solving the model.

homogenized in a few seconds. Furthermore, the air absolute humidity and temperature at the beginning of the simulation are those corresponding to the inlet stream. The Error Objective Function (EOF) to be optimized is defined as the averaged sum of the squared differences between the experimental values of the absolute humidity and temperature of the air at the outlet and those calculated by the model, as shown in the following equation:

$$EOF = \frac{\sum_{k=1}^{N}\left[\left(\frac{y_{g,k}^{calc} - y_{g,k}^{exp}}{y_{g,k}^{calc}}\right)^2 + \left(\frac{T_{g,k}^{calc} - T_{g,k}^{exp}}{T_{g,k}^{calc}}\right)^2\right]}{N} \quad (13)$$

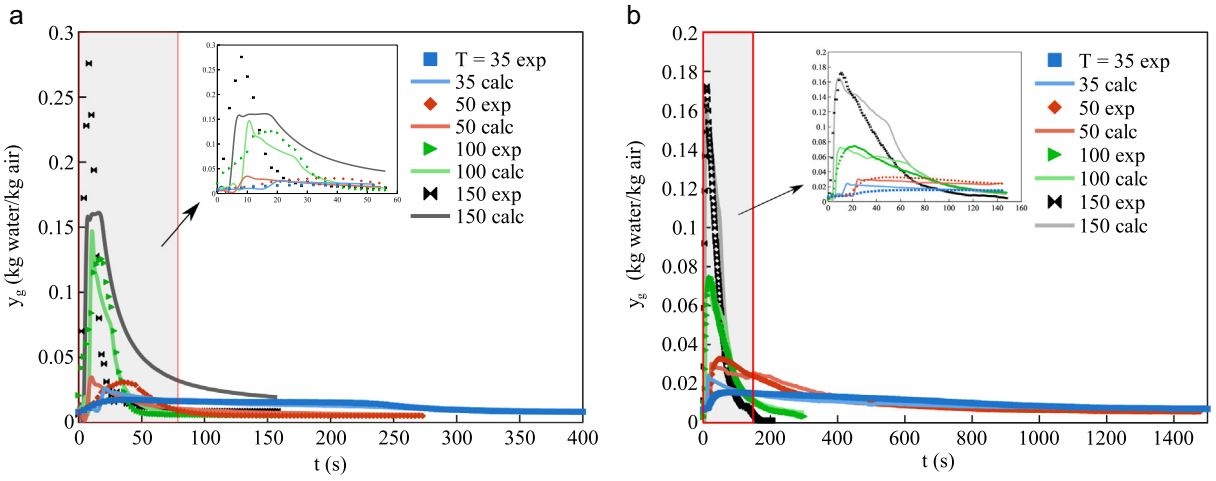

Fig. 7. Evolution of the experimental and calculated outlet air absolute humidity for a) fine and b) ultrafine sand, $u/u_{ms} = 2$.

4. Results and discussion

The model has been designed to estimate the performance of the fountain confined spouted bed dryer, as it allows predicting gas and solid temperatures and moisture contents at different bed zones, as well as those corresponding to the outlet stream. Furthermore, the model is also a tool to determine the overall mass transfer coefficient in the bed. Given that the effect of the operating parameters has been analysed in a previous paper by our research group [63], this one deals with the assessment of a model for the estimation of the drying parameters. Accordingly, the validation of the model is carried out by comparing the calculated values with the experimental ones (bed temperature and outlet air humidity and temperature). The evolution of the experimental and calculated data is shown in Figs. 7 and 8 for an air velocity double the minimum required for spouting, $u/u_{ms} = 2$, as it is the most representative of the air velocities studied.

Overall, the model provides satisfactory predictions for the drying of both fine and ultrafine sands, with EOF values below 0.058. The only significant deviations are observed in the evolution of moisture content when an inlet air temperature of 150 °C is used with the fine sand, Fig. 7a. In this case, the model underestimates the outlet air absolute humidity for the initial drying period and overestimates for the remaining period. This can be explained by the contribution of the hot particles to the evaporation of the water on the surface of the wet particles during the initial drying period. It should be noted that the wet sand was fed onto the annulus, where the wet particles are in close contact with the dry sand particles. In fact, these dry particles are hot (120 °C) at the beginning of the run as shown in Fig. 8. The overestimation of the outlet air absolute humidity for the remaining period is a consequence of the previous underestimation. Given the model cannot predict the contribution of the hot particles to the evaporation of the water on the surface of the wet particles, a lower drying rate is predicted and the critical moisture content is reached later.

Apart from the mentioned deviation, the model faithfully predicts the experimental evolution of air moisture content at the outlet. Thus, Fig. 7 shows that the experimental trends are very similar to the calculated ones except a slight deviation at the beginning of the drying process (the initial peak is sharper than that predicted by the model), which is clearly related to the initial time required in the runs for bed homogenization. This applies especially to the fine sand, Fig. 7a. Thus, the experimental peak is more flattened because drying and homogenization begin at the same time, and therefore the drying efficiency is slightly lower during the homogenization period.

Fig. 8 shows the evolution of the outlet temperature for the solid and the air when the spouting velocity is double the minimum one $u/u_{ms} = 2$. Overall, the model accurately estimates the temperatures for the air and the solid, even though there is a slight discrepancy at the beginning of the operation, which is due to the time required for the homogenization of the pulse of wet sand injected. Furthermore, a comparison of Fig. 8a,c with Fig. 8b,d shows that the outlet air temperature is up to 20 °C lower than the solid temperature at the highest temperature tested, which is mainly explained by the heat loss to the ambient through the wall. This difference decreases as the gas inlet temperature is decreased. The solid features have also a great influence on the process. Thus, the outlet temperature of both air and solid are higher when the drying of fine sands is performed, which is

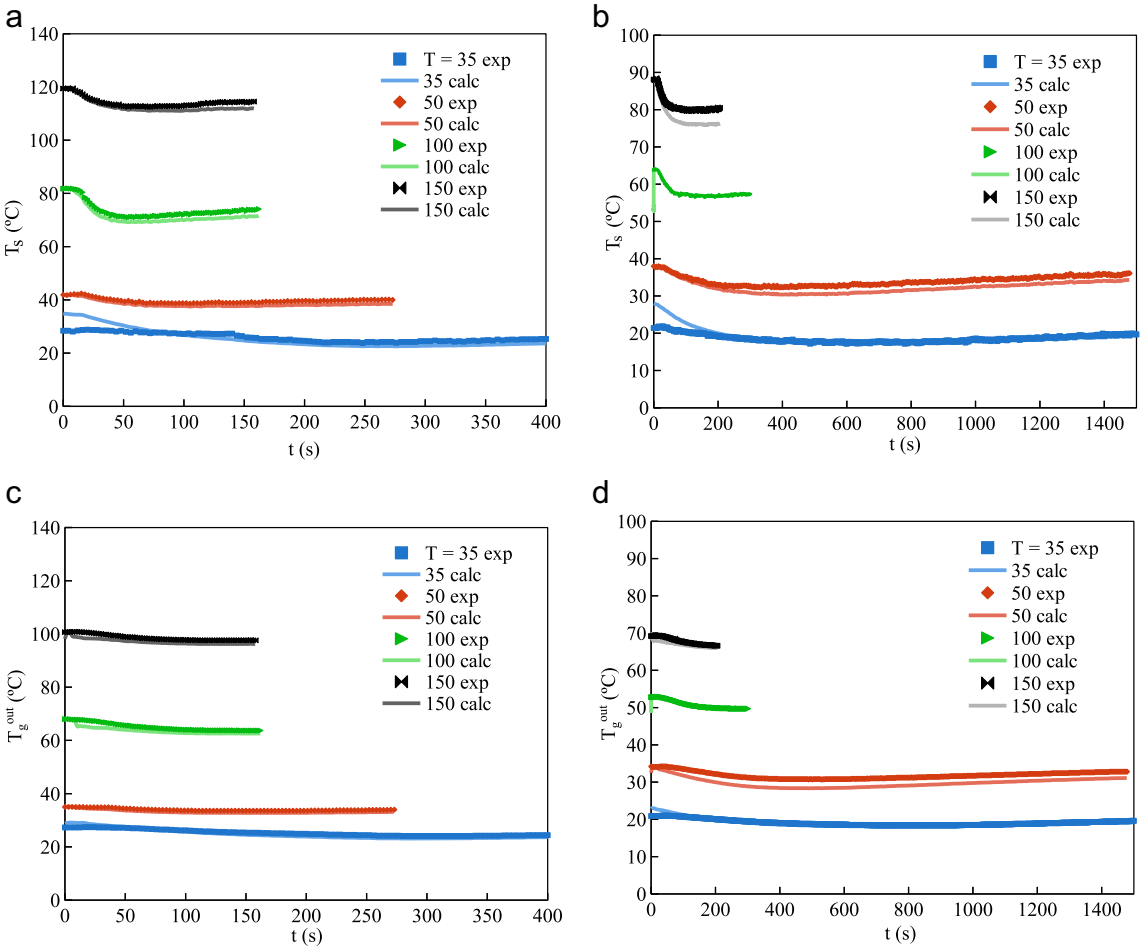

Fig. 8. Evolution of the solid temperature for a) fine, b) ultrafine sands, and outlet air temperature for c) fine and d) ultrafine sands.

explained mainly by the difference in their heat capacities, i.e., 835 and 1105 $J kg^{-1}$ $°C^{-1}$ for the fine and ultrafine sands, respectively.

Fig. 9 shows the values estimated by the model for the mass transfer coefficient in the fountain confined conical spouted bed. The mass transfer coefficient is sensitive to both air inlet temperature and spouting velocity. Thus, the value of the coefficient decreases considerably as the temperature of the inlet air stream is increased. Thus, the highest value of the mass transfer coefficient, $5.7 \cdot 10^{-4}$ ms^{-1}, is found when the fine sand is dried with the highest air flow rate of $u/u_{ms} = 3$ at the lowest inlet air temperature of 35 °C, Fig. 9a. Nevertheless, when the inlet air temperature is increased to 150 °C under the same hydrodynamic condition ($u/u_{ms} = 3$) with this fine sand bed, the value of the mass transfer coefficient decreases to $8.02 \cdot 10^{-6}$ ms^{-1}. This is partially explained by the lower turbulence as temperature is increased. Thus, viscosity increases as temperature is increased, and therefore the Reynolds number decreases. Furthermore, water evaporation due to the close contact of wet particles with dry ones at high temperatures is a relevant mechanism in the annulus, especially at the initial stage in this batch drying process.

Another parameter affecting mass transfer coefficient is the air velocity. Accordingly, for the same inlet air temperature, a decrease in air velocity (lower turbulence) leads to a reduction in the mass transfer coefficient, with differences being smaller as the inlet air temperature is higher. Thus, when an inlet air stream at a temperature of 35 °C is used with fine sand beds, Fig. 9a, the mass transfer coefficient drops from $5.7 \cdot 10^{-4}$ ms^{-1} for an inlet air velocity of $u/u_{ms} = 3$ to $2.4 \cdot 10^{-4}$ ms^{-1} for $u/u_{ms} = 1.2$. This result is due to the lower particle circulation flow rates (longer particle cycle times) as the air velocities are lower [85,94].

Finally, solid properties also affect the mass transfer coefficient, as its values are in general lower for ultrafine sand beds than for fine ones. This is explained by the effect particle size has on the bed performance, i.e., the minimum spouting velocity is lower as particle size is smaller [95–97]. Furthermore, the solid circulation flow rate under the same hydrodynamic conditions (same u/u_{ms}) is higher as the particle size is higher. Another significant difference between the sands used lies in their porosity. Thus, the ultrafine sand is more porous than the fine one, and therefore its interfacial area is larger than that of fine sand. Although a higher area increases the drying rate and consequently the mass transfer, it does not necessary mean a higher drying rate because mass transfer within the particle occurs by diffusion. Ultrafine particles have a higher micropore surface area, which means diffusion prevails, and therefore the overall mass transfer rate is lower.

It should be noted that the general trend changes at high temperatures; that is, mass transfer coefficients are lower for the fine solid than the ultrafine one. This is explained by the different role played by temperature in the drying process depending on whether low or high temperatures are used. Thus, at low temperatures drying occurs mainly by mass transfer through the water/air interphase due to the driving force (saturation moisture content of the air minus the actual content), whereas at high temperatures there is a significant contribution of water evaporation due to particle-particle contact in the annulus.

5. Conclusions

A model based on unsteady heat and mass balances is proposed, which allows predicting the performance of batch drying in a fountain confined conical spouted bed. Furthermore, it is an excellent tool to estimate the overall mass transfer coefficient in these beds. The evolution of the model output parameters, i.e., air humidity and temperature at the outlet, as well as bed temperature, is consistent with the experimental trend, except a slight deviation at the initial stage of the batch drying process, which is related to the time required for the homogenization of the sand particles in the bed.

The parameters affecting the mass transfer coefficient are the air inlet temperature and velocity, as well as solid properties. An increase in the inlet air temperature leads to a decrease in the mass transfer coefficient due to the reduction in the air flow turbulence around the particle. Furthermore, a reduction in the air velocity also leads to a lower mass transfer coefficient, which is attributed to the lower circulation flow rate of both the particles and the air in the bed. Mass transfer rates are higher in the drying of fine sand than ultrafine one. This is explained by both particle size and specific surface area of the sands used. Thus, the size of the fine sand is greater than that of the ultrafine one, and therefore its minimum spouting velocity is higher.

Although operating parameters have proven to be of great influence in the spouted bed dryers at low and moderate temperatures, further research is needed regarding the influence of the geometric factors and high temperatures on the performance of these dryers, and specifically on the role played by the drying mechanisms.

Nomenclature

$\dot{m}_a$	Air mass flow rate, $M\,t^{-1}$
$\dot{m}_s$	Circulation mass flow rate of the solid in the bed, $M\,t^{-1}$
ϵ	Porosity, dimensionless
γ	Cone angle, dimensionless
ω	Fraction of air crossing the nodes, dimensionless
ϕ	Shape factor, dimensionless
ρ_s	Particle density, ML^{-3}

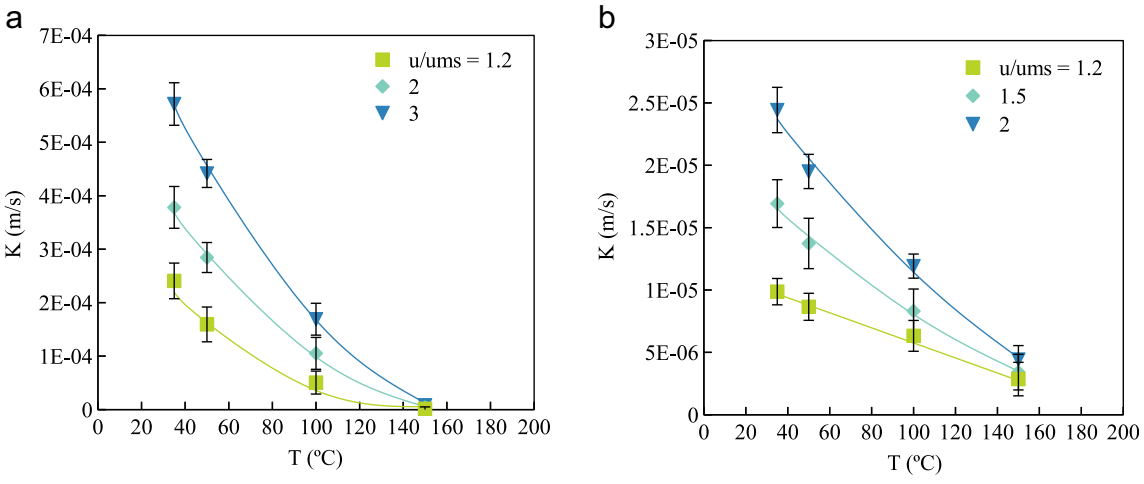

Fig. 9. Effect of operating parameters on the mass transfer coefficient with a) fine sand and b) ultrafine sand.

ρ_b	Bed density, ML^{-3}
a	Gas-solid interphase area, $L^2\ M^{-1}$
A_o	Open area of the draft-tube wall, L^2
A_T	Total area of the draft-tube wall, L^2
C_p	Heat capacity, $L^2\ t^{-2}\ T^{-1}$
D_c	Diameter of the cylindrical section, L
D_F	Diameter of the fountain confiner, L
D_i	Contactor base diameter, L
D_o	Gas inlet diameter, L
d_p^v	Volume average particle size, L
d_p^w	Mass average particle size, L
D_T	Internal diameter of the draft-tube, L
H_c	Height of the conical section, L
h_c	Instantaneous heat transfer coefficient, $Mt\ L^{-2}$
H_F	Distance between the bed surface and the fountain confiner, L
H_o	Static bed height, L
h_s	Enthalpy of the solid, $L^2\ t^{-2}$
h_v	Enthalpy of the steam, $L^2\ t^{-2}$
h_w	Enthalpy of the liquid water, $L^2\ t^{-2}$
K	Overall mass transfer coefficient, $L\ t^{-1}$
L_F	Length of the fountain confiner, L
L_H	Solid entrainment height at the lower section of the draft-tube, L
L_T	Length of the draft-tube, L
M_g	Amount of air in the nodes, M
M_s	Amount of solid in the nodes, M
R_w	Drying rate, $M\ t^{-1}$
T_g	Air temperature, T
T_i	Inlet air temperature, T
T_s	Solid temperature, T
T_{amb}	Ambient temperature, T
u_g	Air velocity, $L\ t^{-1}$
U_oA_o	Heat transfer coefficient through the wall, $M\ t$
u_{ms}	Minimum spouting velocity, $L\ t^{-1}$
V	Volume of the nodes, L^3
x_s	Moisture content in the nodes, dimensionless
x_s^c	Critical solid moisture, dimensionless
y_g	Air absolute humidity, dimensionless
y_{sat}	Saturation absolute humidity, dimensionless
EOF	Error Objective Function

Credit authorship contribution statement

Xabier Sukunza: Investigation, Software, Writing – original draft, Visualization. **Aitor Pablos:** Methodology, Investigation, Formal analysis, Project administration. **Mikel Tellabide:** Data curation, Formal analysis, Conceptualization, Project administration. **Idoia Estiati:** Validation, Formal analysis. **Fábio Bentes Freire:** Validation, Formal analysis. **Roberto Aguado:** Conceptualization, Resources, Writing – review & editing, Visualization, Supervision, Funding acquisition. **Martin Olazar:** Conceptualization, Resources, Writing – review & editing, Supervision, Funding acquisition.

Declaration of Competing Interest

The authors declare that they have no known competing financial interests or personal relationships that could have appeared to influence the work reported in this paper.

Acknowledgments

This work has received funding from Spain's Ministry of Science and Innovation (PID2019-107357RB-I00 (AEI/FEDER, UE), PLE2021-008062 (European Union NextGenerationEU/PRTR)) and the European Commission (HORIZON H2020-MSCA RISE-2018, Contract No.: 823745). The authors thank the technical and human support provided by IZO-SGI SGIker from University of the Basque Country UPV/EHU and European funding (ERDF and ESF). Xabier Sukunza thanks the Ministry of Economy and Competitiveness for his Ph.D. grant (FPU18/04935). Idoia Estiati is grateful for her postgraduate grant (ESPDOC18/14) from the University of the Basque Country UPV/EHU.

References

[1] P. E. Gishler, K. B. Mathur, Method of contacting solid particles with fluids. Patente: US2786280 (A) (jul 1957).
[2] L.N. Kahyaoglu, S. Sahin, G. Sumnu, Spouted bed and microwave-assisted spouted bed drying of parboiled wheat, Food Bioprod. Process. 90 (2) (2012) 301–308, https://doi.org/10.1016/j.fbp.2011.06.003.
[3] W. Jittanit, G. Srzednicki, R. Driscoll, Seed drying in fluidized and spouted bed dryers, Dry. Technol. 28 (10) (2010) 1213–1219, https://doi.org/10.1080/07373937.2010.483048.
[4] S. Hamedi, M.M. Afsahi, M.H. Nematollahi, H.R. Akhavan, Spouted bed drying of skimmed milk: multivariable optimization of the conditions to improve physico-chemical properties of the dried milk, LWT 146 (2021), 111448, https://doi.org/10.1016/j.lwt.2021.111448.
[5] A. Magalhães, C. Pinho, Spouted bed drying of cork stoppers, Chem. Eng. Process. Process Intensif. 47 (12) (2008) 2395–2401, https://doi.org/10.1016/j.cep.2007.11.009.
[6] M. Zielinska, M. Markowski, Drying behavior of carrots dried in a spout-fluidized bed dryer, Dry. Technol. 25 (1) (2007) 261–270, https://doi.org/10.1080/07373930601161138.
[7] M.G. Rasul, Spouted bed combustion of wood charcoal: performance comparison of three different designs, Fuel 80 (15) (2001) 2189–2191, https://doi.org/10.1016/S0016-2361(01)00110-7.
[8] Q. Wang, X. Kong, H. Liu, G. Xiao, Combustion experimental study on spouted bed for daqing oil shale semi-coke, Advanced Materials Research, vol. 614–615, Trans Tech Publications Ltd 2013, pp. 95–98.
[9] D.O. Albina, Combustion of rice husk in a multiple-spouted fluidized bed, Energy Sources 25 (9) (2003) 893–904, https://doi.org/10.1080/00908310390212246.
[10] H. Boujjat, S. Rodat, S. Chuayboon, S. Abanades, Experimental and numerical study of a directly irradiated hybrid solar/combustion spouted bed reactor for continuous steam gasification of biomass, Energy 189 (2019), 116118, https://doi.org/10.1016/j.energy.2019.116118.
[11] H.C. Park, B.K. Lee, H.S. Yoo, H.S. Choi, [TC2015] fast pyrolysis characteristics of biomass in a conical spouted bed reactor, Environmental Progress and Sustainable Energy 36 (3) (2017) 685–689, https://doi.org/10.1002/ep.12476.
[12] H.C. Park, B.K. Lee, H.S. Yoo, H.S. Choi, Influence of operating conditions for fast pyrolysis and pyrolysis oil production in a conical spouted-bed reactor, Chem. Eng. Technol. 42 (12) (2019) 2493–2504, https://doi.org/10.1002/ceat.201900082.
[13] A. Niksiar, A.H. Faramarzi, M. Sohrabi, Kinetic study of polyethylene terephthalate (PET) pyrolysis in a spouted bed reactor, J. Anal. Appl. Pyrolysis 113 (2015) 419–425, https://doi.org/10.1016/j.jaap.2015.03.002.
[14] K.M. Barcelos, P.S. Almeida, M.S. Araujo, T.P. Xavier, K.G. Santos, M.S. Bacelos, T.S. Lira, Particle segregation in spouted bed pyrolysis reactor: sand-coconut shell and sand-cocoa shell mixtures, Biomass Bioenergy 138 (2020), 105592, https://doi.org/10.1016/j.biombioe.2020.105592.
[15] D.Z. Mantegazini, T.P. Xavier, M.S. Bacelos, Conical spouted beds for waste valorization: assessment of particle segregation in beds composed of sand and tetra Pak residues, Sustainable Energy Technologies and Assessments 47 (2021), 101334, https://doi.org/10.1016/j.seta.2021.101334.
[16] Z. Wang, C.J. Lim, J.R. Grace, Biomass torrefaction in a slot-rectangular spouted bed reactor, Particuology 42 (2019) 154–162, https://doi.org/10.1016/j.partic.2018.02.002.
[17] W.Y. Chen, H.P. Kuo, Surface coating of group B iron powders in a spouted bed, Procedia Engineering, vol. 102, Elsevier Ltd 2015, pp. 1144–1149, https://doi.org/10.1016/j.proeng.2015.01.238.
[18] J.L. Vieira Neto, J.E. Borges, C.R. Duarte, M.A. Barrozo, Coating of particles in spouted bed: flow regime and stability, Materials Science Forum, vol. 660–661, Trans Tech Publications Ltd 2010, pp. 573–579.
[19] S. Rajashekhara, D.V.R. Murthy, Drying of agricultural grains in a multiple porous draft tube spouted bed, Chem. Eng. Commun. 204 (8) (2017) 942–950, https://doi.org/10.1080/00986445.2017.1328412.
[20] R.C. Brito, M.B. Zacharias, V.A. Forti, J.T. Freire, Physical and physiological quality of intermittent soybean seeds drying in the spouted bed, Dry. Technol. 39 (6) (2021) 820–833, https://doi.org/10.1080/07373937.2020.1725544.
[21] R.C. Brito, R. Béttega, J.T. Freire, Energy analysis of intermittent drying in the spouted bed, Dry. Technol. 37 (12) (2019) 1498–1510, https://doi.org/10.1080/07373937.2018.1512503.
[22] I. Estiati, M. Tellabide, J.F. Saldarriaga, H. Altzibar, M. Olazar, Influence of the fountain confiner in a conical spouted bed dryer, Powder Technol. 356 (2019) 193–199, https://doi.org/10.1016/j.powtec.2019.08.005.
[23] X. Sukunza, A. Pablos, R. Aguado, J. Vicente, H. Altzibar, M. Olazar, Continuous drying of fine and ultrafine sands in a fountain confined conical spouted bed, Powder Technol. 388 (2021) 371–379, https://doi.org/10.1016/j.powtec.2021.04.081.
[24] C.A. Moreira da Silva, M.D.C. Ferreira, F.B. Freire, J.T. Freire, Analysis of the dynamics of paste drying in a spouted bed, Drying Technology 37 (7) (2019) 876–884, https://doi.org/10.1080/07373937.2018.1471699.
[25] J.T. Freire, F.B. Freire, M.C. Ferreira, B.S. Nascimento, A hybrid lumped parameter/neural network model for spouted bed drying of pastes with inert particles, Dry.

Technol. 30 (11−12) (2012) 1342–1353, https://doi.org/10.1080/07373937.2012.684085.
[26] S.T.C. Tangsatitkulchai, P. Dumronglaohapun, Continuous drying of slurry in a jet spouted bed, Dry. Technol. 13 (8–9) (1995) 1825–1840, https://doi.org/10.1080/07373939508917053.
[27] M.H. El-Naas, S. Rognon, R. Legros, R.C. Mayer, Hydrodynamics and mass transfer in a spouted bed dryer, Dry. Technol. 18 (1–2) (2000) 323–340, https://doi.org/10.1080/07373930008917707.
[28] H. Becker, H. Sallans, Drying wheat in a spouted bed. On the continuous, moisture diffusion controlled drying of solid particles in a well-mixed, isothermal bed, Chemical Engineering Science 13 (3) (1960) 97–112.
[29] A.H. Zahed, N. Epstein, Batch and Continuous Spouted Bed Drying of Cereal Grains: The Thermal Equilibrium Model, Oct 1992 https://doi.org/10.1002/cjce.5450700517.
[30] A.H. Zahed, N. Enstein, On the diffusion mechanism during spouted bed drying of cereal grains, Dry. Technol. 11 (2) (1993) 401–409, https://doi.org/10.1080/07373939308916827.
[31] C. Zuritz, R. Singh, Simulation of Rough Rice in a Spouted-Bed, McGraw-Hill Hemisphere, 1982 239–247.
[32] T. Madhiyanon, S. Soponronnarit, W. Tia, A two-region mathematical model for batch drying of grains in a two-dimensional spouted bed, Dry. Technol. 19 (6) (2001) 1045–1064, https://doi.org/10.1081/DRT-100104804.
[33] M. Markowski, I. Białobrzewski, A. Modrzewska, Kinetics of spouted-bed drying of barley: diffusivities for sphere and ellipsoid, J. Food Eng. 96 (3) (2010) 380–387, https://doi.org/10.1016/j.jfoodeng.2009.08.011.
[34] W.B. Bie, G. Srzednicki, R.H. Driscoll, Study of temperature and moisture distribution in paddy in a triangular spouted bed dryer, Dry. Technol. 25 (1) (2007) 177–183, https://doi.org/10.1080/07373930601161062.
[35] A. Go, S.K. Das, G. Srzednicki, R.H. Driscoll, Modeling of moisture and temperature changes of wheat during drying in a triangular spouted bed dryer, Dry. Technol. 25 (4) (2007) 575–580, https://doi.org/10.1080/07373930701227060.
[36] N.V. Men'shutina, A.E. Korneeva, H. Leuenberger, Modeling of atmospheric freeze drying in a spouted bed, Theor. Found. Chem. Eng. 39 (6) (2005) 594–598, https://doi.org/10.1007/s11236-005-0122-4.
[37] J.T. Freire, M.C. Ferreira, F.B. Freire, B.S. Nascimento, A review on paste drying with inert particles as support medium, Dry. Technol. 30 (4) (2012) 330–341, https://doi.org/10.1080/07373937.2011.638149.
[38] R.C. Brito, R.C. Sousa, R. Béttega, F.B. Freire, J.T. Freire, Analysis of the energy performance of a modified mechanically spouted bed applied in the drying of alumina and skimmed milk, Chemical Engineering and Processing - Process Intensification 130 (2018) 1–10, https://doi.org/10.1016/j.cep.2018.05.014.
[39] W.P. Oliveira, J.T. Freire, Analysis of evaporating rate in the spouted bed zones during drying of liquid materials using a three region model, Proc. of the 10th Intern. Drying Symp. (IDS'96), Cracow, Poland 1996, pp. 504–512.
[40] B.S. Nascimento, F.B. Freire, J.T. Freire, Moisture prediction during paste drying in a spouted bed, Dry. Technol. 31 (15) (2013) 1808–1816, https://doi.org/10.1080/07373937.2013.825627.
[41] Y.M. da Silva Veloso, M.M. de Almeida, O.L.S. de Alsina, M.S. Leite, Artificial neural network model for the flow regime recognition in the drying of guava pieces in the spouted bed, Chem. Eng. Commun. 207 (4) (2020) 549–558, https://doi.org/10.1080/00986445.2019.1608192.
[42] K.B. Park, J.L. Plawsky, H. Littman, J.D. Paccione, Mortar properties obtained by dry premixing of cementitious materials and sand in a spout-fluid bed mixer, Cem. Concr. Res. 36 (4) (2006) 728–734, https://doi.org/10.1016/j.cemconres.2005.10.012.
[43] J.L. Plawsky, S. Jovanovic, H. Littman, K.C. Hover, S. Gerolimatos, K. Douglas, Exploring the effect of dry premixing of sand and cement on the mechanical properties of mortar, Cement and Concrete Research, vol. 33, Pergamon 2003, pp. 255–264, https://doi.org/10.1016/S0008-8846(02)00927-4.
[44] M. Olazar, M.J. San José, A.T. Aguayo, J.M. Arandes, J. Bilbao, Stable operation conditions for gas-solid contact regimes in conical spouted beds, Ind. Eng. Chem. Res. 31 (7) (1992) 1784–1792, https://doi.org/10.1021/ie00007a025.
[45] L. Zhang, Z. Wang, S. Li, H. Qin, Effect of a draft tube on oil shale particle drying process of a spouted bed: CPFD simulation studies, Adv. Powder Technol. 29 (9) (2018) 2255–2267, https://doi.org/10.1016/j.apt.2018.06.010.
[46] J.L. Vieira Neto, C.R. Duarte, V.V. Murata, M.A. Barrozo, Effect of a draft tube on the fluid dynamics of a spouted bed: experimental and CFD studies, Dry. Technol. 26 (3) (2008) 299–307, https://doi.org/10.1080/07373930801897994.
[47] H. Altzibar, G. Lopez, S. Alvarez, M.J. San Jose, A. Barona, M. Olazar, A draft-tube conical spouted bed for drying fine particles, Dry. Technol. 26 (3) (2008) 308–314, https://doi.org/10.1080/07373930801898018.
[48] M. Olazar, G. Lopez, H. Altzibar, J. Bilbao, Modelling batch drying of sand in a draft-tube conical spouted bed, Chem. Eng. Res. Des. 89 (10) (2011) 2054–2062, https://doi.org/10.1016/j.cherd.2011.01.012.
[49] H. Altzibar, M. Tellabide, I. Estiati, M. Olazar, Effect of a device for retaining solids on the fountain height in the nonporous draft tube conical spouted bed, chemical, Eng. Trans. 57 (2017) 847–852, https://doi.org/10.3303/CET1757142.
[50] I. Estiati, M. Tellabide, A. Pablos, H. Altzibar, R. Aguado, M. Olazar, Design factors in fountain confined conical spouted beds, Chemical Engineering and Processing - Process Intensification 155 (2020), 108062, https://doi.org/10.1016/j.cep.2020.108062.
[51] X. Sukunza, A. Pablos, R. Aguado, J. Vicente, J. Bilbao, M. Olazar, Effect of the solid inlet design on the continuous drying of fine and ultrafine sand in a fountain confined conical spouted bed, Ind. Eng. Chem. Res. 59 (19) (2020) 9233–9241, https://doi.org/10.1021/acs.iecr.0c00575.
[52] M. Tellabide, I. Estiati, A. Pablos, H. Altzibar, R. Aguado, M. Olazar, New operation regimes in fountain confined conical spouted beds, Chem. Eng. Sci. 211 (2020), 115255https://doi.org/10.1016/j.ces.2019.115255.
[53] A. Kmiec, Simultaneous heat and mass transfer in spouted beds, Can. J. Chem. Eng. 53 (1) (1975) 18–24, https://doi.org/10.1002/cjce.5450530103.
[54] R.G. Szafran, A. Kmiec, CFD modeling of heat and mass transfer in a spouted bed dryer, Ind. Eng. Chem. Res. 43 (4) (2004) 1113–1124, https://doi.org/10.1021/ie0305824.
[55] T. Hoffmann, A.H. Bedane, M. Peglow, E. Tsotsas, M. Jacob, Particle-gas mass transfer in a spouted bed with adjustable air inlet, Dry. Technol. 29 (3) (2011) 257–265, https://doi.org/10.1080/07373937.2010.483046.
[56] J.F. Saldarriaga, R. Aguado, A. Atxutegi, J. Grace, J. Bilbao, M. Olazar, Correlation for calculating heat transfer coefficient in conical spouted beds, Ind. Eng. Chem. Res. 55 (35) (2016) 9524–9532, https://doi.org/10.1021/acs.iecr.6b02234.
[57] O. Yaman, G. Kulah, M. Koksal, Surface-to-bed heat transfer for high-density particles in conical spouted and spout-fluid beds, Particuology 42 (2019) 35–47, https://doi.org/10.1016/j.partic.2018.03.013.
[58] J. Bandrowski, G. Kaczmarzyk, Gas-to-particle heat transfer in vertical pneumatic conveying of granular materials, Chem. Eng. Sci. 33 (10) (1978) 1303–1310, https://doi.org/10.1016/0009-2509(78)85111-2.
[59] S.C. Rocha, O.P. Taranto, G.E. Ayub, Aerodynamics and heat transfer during coating of tablets in two-dimensional spouted bed, Can. J. Chem. Eng. 73 (3) (1995) 308–312, https://doi.org/10.1002/cjce.5450730306.
[60] F. Ronsse, J.G. Pieters, K. Dewettinck, Numerical spray model of the fluidized bed coating process, Dry. Technol. 25 (9) (2007) 1491–1514, https://doi.org/10.1080/07373930701537245.
[61] F. Ronsse, J.G. Pieters, K. Dewettinck, Modelling heat and mass transfer in batch, top-spray fluidised bed coating processes, Powder Technol. 190 (1–2) (2009) 170–175, https://doi.org/10.1016/j.powtec.2008.04.048.
[62] A. Kmiec, S. Englart, A. Ludwinska, Mass transfer during air humidification in spouted beds, Can. J. Chem. Eng. 87 (2) (2009) 163–168, https://doi.org/10.1002/cjce.20152.
[63] A. Pablos, R. Aguado, J. Vicente, H. Altzibar, J. Bilbao, M. Olazar, Effect of operating conditions on the drying of fine and ultrafine sand in a fountain confined conical spouted bed, Dry. Technol. 38 (11) (2020) 1446–1461, https://doi.org/10.1080/07373937.2019.1645684.
[64] R. Brown, J. Richards, Principles of Powder Mechanics, 1st edition Pergamon Press, Oxford, 1970.
[65] A. Pablos, R. Aguado, J. Vicente, M. Tellabide, J. Bilbao, M. Olazar, Elutriation, attrition and segregation in a conical spouted bed with a fountain confiner, Particuology (2022) https://doi.org/10.1016/j.partic.2019.08.006.
[66] A. Pablos, R. Aguado, M. Tellabide, H. Altzibar, F.B. Freire, J. Bilbao, M. Olazar, A new fountain confinement device for fluidizing fine and ultrafine sands in conical spouted beds, Powder Technol. 328 (2018) 38–46, https://doi.org/10.1016/j.powtec.2017.12.090.
[67] I. Estiati, M. Tellabide, J.F. Saldarriaga, H. Altzibar, M. Olazar, Fine particle entrainment in fountain confined conical spouted beds, Powder Technol. 344 (2019) 278–285, https://doi.org/10.1016/j.powtec.2018.12.035.
[68] M.M. Choi, A. Meisen, Sulfur coating of urea in shallow spouted beds, Chem. Eng. Sci. 52 (7) (1997) 1073–1086, https://doi.org/10.1016/S0009-2509(96)00377-6.
[69] A. Pablos, M. Tellabide, I. Estiati, J. Vicente, R. Aguado, M. Olazar, Modelling batch drying of fine sand in a fountain confined conical spouted bed, IDS2018. 21st International Drying Symposium, Valencia, Spain 2018, pp. 1623–1630, https://doi.org/10.4995/ids2018.2018.7543.
[70] L. Spreutels, B. Haut, J. Chaouki, F. Bertrand, R. Legros, Conical spouted bed drying of Baker's yeast: experimentation and multi-modeling, Food Res. Int. 62 (2014) 137–150, https://doi.org/10.1016/j.foodres.2014.02.027.
[71] Y. Du, Q. Yang, A.S. Berrouk, C. Yang, A.S. Al Shoaibi, Equivalent reactor network model for simulating the air gasification of polyethylene in a conical spouted bed gasifier, Energy Fuel 28 (11) (2014) 6830–6840, https://doi.org/10.1021/ef501667n.
[72] F. Marchelli, C. Moliner, M. Curti, B. Bosio, E. Arato, Cfd-dem simulations of a continuous square-based spouted bed and evaluation of the solids residence time distribution, Powder Technol. 366 (2020) 840–858, https://doi.org/10.1016/j.powtec.2020.03.017.
[73] L. Spreutels, J. Chaouki, F. Bertrand, B. Haut, R. Legros, Gas residence time distribution in a conical spouted bed, Powder Technol. 290 (2016) 62–71, https://doi.org/10.1016/j.powtec.2015.07.033.
[74] R.G. Szafran, A. Kmiec, W. Ludwig, CFD modeling of a spouted-bed dryer hydrodynamics, Dry. Technol. 23 (8) (2005) 1723–1736, https://doi.org/10.1081/DRT-200065179.
[75] N. Epstein, J.R. Grace, Spouted and Spout-Fluid Beds: Fundamentals and Applications, vol. 9780521517, Cambridge University Press, 2010 https://doi.org/10.1017/CBO9780511777936.
[77] W. Shuyan, H. Zhenghua, S. Dan, L. Yikun, W. Lixin, W. Shuai, Hydrodynamic Simulations of Gas-Solid Spouted Bed with a Draft Tube, feb 2010 https://doi.org/10.1016/j.ces.2009.09.060.
[78] H. Nagashima, T. Ishikura, M. Ide, Effect of the tube shape on gas and particle flow in spouted beds with a porous draft tube, Can. J. Chem. Eng. 87 (2) (2009) 228–236, https://doi.org/10.1002/cjce.20150.
[79] T. Ishikura, H. Nagashima, M. Ide, Hydrodynamics of a spouted bed with a porous draft tube containing a small amount of finer particles, Powder Technol. 131 (1) (2003) 56–65, https://doi.org/10.1016/S0032-5910(02)00321-2.
[80] F.G. Cunha, K.G. Santos, C.H. Ataíde, N. Epstein, M.A. Barrozo, Annatto powder production in a spouted bed: an experimental and CFD study, Ind. Eng. Chem. Res. 48 (2) (2009) 976–982, https://doi.org/10.1021/ie801382d.

[81] N. Dogan, M. Koksal, G. Kulah, Gas velocity distribution in conical spouted beds with high-density particles, Can. J. Chem. Eng. 99 (7) (2021) 1607–1615, https://doi.org/10.1002/cjce.24012.
[82] M.S. Bacelos, P.I. Almeida, Modelling of drying kinetic of potatoes taking into account shrinkage, Procedia Food Science 1 (2011) 713–721, https://doi.org/10.1016/j.profoo.2011.09.108.
[83] I. Estiati, M. Tellabide, J.F. Saldarriaga, H. Altzibar, F.B. Freire, J.T. Freire, M. Olazar, Comparison of artificial neural networks with empirical correlations for estimating the average cycle time in conical spouted beds, Particuology 42 (2019) 48–57, https://doi.org/10.1016/j.partic.2018.03.010.
[84] I. Estiati, A. Atxutegi, H. Altzibar, F.B. Freire, R. Aguado, M. Olazar, Multiple-output artificial neural network to estimate solid cycle times in conical spouted beds, Chem. Eng. Technol. 44 (3) (2021) 542–550, https://doi.org/10.1002/ceat.202000491.
[85] J.F. Saldarriaga, I. Estiati, A. Atxutegi, R. Aguado, J. Bilbao, M. Olazar, Distribution of cycle times in sawdust conical spouted bed equipped with fountain confiner and draft tube, Ind. Eng. Chem. Res. 58 (5) (2019) 1932–1940, https://doi.org/10.1021/acs.iecr.8b03451.
[86] I. Estiati, H. Altzibar, M. Tellabide, M. Olazar, A new method to measure fine particle circulation rates in draft tube conical spouted beds, Powder Technology 316 (2017) 87–91 , fluidization for Emerging Green Technologies https://doi.org/10.1016/j.powtec.2017.01.040.
[87] M. Olazar, M.J. San Jose, M.A. Izquierdo, S. Alvarez, J. Bilbao, Local bed voidage in spouted beds, Industrial & Engineering Chemistry Research 40 (1) (2001) 427–433.
[88] M. Tellabide, I. Estiati, A. Atxutegi, H. Altzibar, R. Aguado, M. Olazar, Fine particle flow pattern and region delimitation in fountain confined conical spouted beds, J. Ind. Eng. Chem. 95 (2021) 312–324, https://doi.org/10.1016/j.jiec.2021.01.006.
[89] R.C. de Brito, M. Tellabide, A. Atxutegi, I. Estiati, J.T. Freire, M. Olazar, Draft tube design based on a borescopic technique in conical spouted beds, Adv. Powder Technol. 32 (11) (2021) 4420–4431, https://doi.org/10.1016/j.apt.2021.10.004.
[90] W.J. Coumans, Models for drying kinetics based on drying curves of slabs, Chem. Eng. Process. Process Intensif. 39 (1) (2000) 53–68, https://doi.org/10.1016/S0255-2701(99)00084-7.
[91] P. Rowe, K. Claxton, Heat and mass transfer from a single sphere to fluid flowing through an array, Trans. Inst. Chem. Eng. 43 (10) (1965) 321–331.
[92] A.M. Keech, R.B. Keey, Q.J. Zhang, T.A. Langrish, I.C. Kemp, H.S. Pasley, An experimental test of the concept of the characteristic drying curve using the thin-layer method, Dry. Technol. 13 (5–7) (1995) 1133–1152, https://doi.org/10.1080/07373939508917013.
[93] J.A. Nelder, R. Mead, A simplex method for function minimization, Comput. J. 7 (4) (1965) 308–313, https://doi.org/10.1093/comjnl/7.4.308.
[94] M.J. San José, M. Olazar, M.A. Izquierdo, S. Alvarez, J. Bilbao, Solid trajectories and cycle times in spouted beds, Ind. Eng. Chem. Res. 43 (13) (2004) 3433–3438, https://doi.org/10.1021/ie030668x.
[95] M. Tellabide, I. Estiati, A. Pablos, H. Altzibar, R. Aguado, M. Olazar, Minimum spouting velocity of fine particles in fountain confined conical spouted beds, Powder Technol. 374 (2020) 597–608, https://doi.org/10.1016/j.powtec.2020.07.087.
[96] S.H. Hosseini, M.J. Rezaei, M. Bag-Mohammadi, H. Altzibar, M. Olazar, Smart models to predict the minimum spouting velocity of conical spouted beds with non-porous draft tube, Chem. Eng. Res. Des. 138 (2018) 331–340, https://doi.org/10.1016/j.cherd.2018.08.034.
[97] H. Altzibar, G. Lopez, J. Bilbao, M. Olazar, Minimum spouting velocity of conical spouted beds equipped with draft tubes of different configuration, Ind. Eng. Chem. Res. 52 (8) (2013) 2995–3006, https://doi.org/10.1021/ie302407f.